EXTENSION OF EARTH ORBITS USING LOW-THRUST PROPULSION

Ms. Pamela Anderson
Advanced Space Concepts Laboratory University of Strathclyde, Glasgow, United Kingdom,
pamela.c.anderson@strath.ac.uk

Dr. Malcolm Macdonald
Advanced Space Concepts Laboratory University of Strathclyde, Glasgow, United Kingdom,
malcolm.macdonald.102@strath.ac.uk

The primary motivation for the utilization of space for environmental science, and in-particular Earth Observation, is the unique vantage point which a spacecraft can provide. For example, a spacecraft can provide a global dataset with a much higher temporal resolution than any other platform.

Earth Observation spacecraft are increasingly focused on a single primary application, typically conducted from a small set of classical orbits which limits the range of vantage points and hence the type of observations which can be made. The next generation of innovative Earth Observation spacecraft may however only be enabled through new orbit options not considered in the past. The objective of the study was therefore to enlarge the set of potential Earth orbits by considering the use of low-thrust propulsion to extend the conventional Molniya orbit. These new orbits will use existing, or near-term low-thrust propulsion technology to enable new Earth Observation science and offer a radically new set of tools for mission design.

Continuous low-thrust propulsion was applied in the radial, transverse and normal directions to vary the critical inclination of the Molniya orbit, while maintaining the zero change in argument of perigee condition. As such the inclination can be freely altered from the expected critical inclination of 63.4 deg, to, for example 90 deg, creating a Polar-Molniya orbit. Analytical expressions were developed which were then validated using a numerical model, to show that not only was the argument of perigee unchanged but all other orbital elements were also unaffected by the applied low-thrust.

It was shown that thrusting in the transverse direction allowed the spacecraft to achieve any inclination with the lowest thrust magnitude in any single direction; this value was however found to be further reduced by combining both radial and transverse thrust. Real-time continuous observation of the Arctic Circle is then enabled using current electric propulsion technology, with fewer spacecraft than the traditional Sun-synchronous polar orbit, and at reduced range than a 'pole-sitter'. Applications of such an orbit would include more accurate Arctic weather predictions and severe weather event warnings for this region.

I. NOMENCLATURE

a	=	semi-major axis
$C_{n,m}$	=	harmonic coefficients of Earth potential
e	=	eccentricity
F_n	=	low-thrust normal perturbation scalar
F_r	=	low-thrust radial perturbation scalar
F_t	=	low-thrust transverse perturbation scalar
i	=	inclination
J_2	=	perturbation due to Earth oblateness
N	=	normal perturbation force
p	=	semi-parameter
$P_{n,m}$	=	associated Legendre polynomials
r	=	orbit radius
R	=	radial perturbation force
R_e	=	mean radius of Earth
$S_{n,m}$	=	harmonic coefficients of Earth potential
T	=	transverse perturbation force
U	=	potential
U_o	=	point-mass gravitational potential
U_p	=	perturbing component of potential body
β	=	declination of spacecraft
θ	=	true anomaly
λ	=	geographical longitude
μ	=	gravitational parameter of Earth
ω	=	argument of perigee
Ω	=	ascending node angle

SI Units used throughout unless otherwise stated.

II. INTRODUCTION

Spacecraft provide a unique platform from which to view the Earth and conduct environmental science, offering higher temporal resolution, on a global scale than any other method. Consequently, space-based Earth Observation (EO) measurements for climate change and other monitoring applications are of fundamental importance for validation and assimilation into Earth system models; the Committee on Earth Observation Satellites (CEOS) and the Global Climate Observing System (GCOS) has identified 21 Essential Climate Variables (ECVs) that are largely dependent on space-based EO [1]. However, it is of note that the vantage points currently used by spacecraft for environmental science and EO represent only a small subset of those available. Consequently, the aim of this study is to examine the use of low-thrust propulsion applied to conventional orbits to produce novel orbits to enable new EO mission design in a similar manner to the extension of the Sun-synchronous orbit for free selection of orbit inclination and altitude using low-thrust propulsion [2].

The Molniya orbit is a type of highly elliptical orbit, with a period, typically, of one half of a sidereal day, characteristic of the Molniya orbit is the fixed *63.4deg* or *116.6deg* inclination [3]. At either of these critical inclinations the argument of perigee no longer rotates due to the concentration of mass around the Earths equator, and the position of apogee remains unchanged. Applications of spacecraft on the Molniya orbit are generally used for communication over high latitude regions of the Earth and offer a unique vantage of the polar regions [4]. Consideration is given to the application of low-thrust to change the critical inclination of the orbit. Analytical expressions will be developed, which will then be validated within an independently generated numerical model.

III. SATELLITE MOTION ABOUT AN OBLATE BODY

The gravitational potential [5] may be written as,

$$U(r,\beta,\lambda)=\frac{\mu}{r}\sum_{n=0}^{\infty}\sum_{m=0}^{\infty}\left(\frac{R_e}{r}\right)^n (C_{n,m}Cosm\lambda+S_{n,m}Sinm\lambda)P_{n,m}Sin\beta \qquad [1]$$

For a body possessing axial symmetry the influence of periodic effects (tesseral and sectorial harmonics) can be neglected for most orbits, with the notable exception of geostationary orbits this is true for Earth. The gravitational potential may then be written as,

$$U(r,\beta)=\frac{\mu}{r}\left[1-\sum_{n=0}^{\infty}J_n\left(\frac{R_e}{r}\right)^n P_nSin\beta\right] \qquad [2]$$

Expanding Equation [2], the gravitational potential becomes,

$$\begin{aligned}U(r,\beta)=\frac{\mu}{r}[1&-J_2\frac{1}{2}\left(\frac{R_e}{r}\right)^2\left(3Sin^2\beta-1\right)\\&-J_3\frac{1}{2}\left(\frac{R_e}{r}\right)^3\left(5Sin^2\beta-3\right)Sin\beta\\&-J_4\frac{1}{8}\left(\frac{R_e}{r}\right)^4\left(3-30Sin^2\beta+35Sin^4\beta\right)\\&-........]\end{aligned} \qquad [3]$$

Considering only first order perturbations and using spherical triangle laws Equation [3] becomes,

$$\begin{aligned}U(r,\beta)&=U_o+U_p\\&=\frac{\mu}{r}-J_2\frac{\mu R_e^2}{2r^3}(3Sin^2iSin^2(\theta+\omega)-1)\end{aligned} \qquad [4]$$

The argument of perigee must remain unchanged in order to ensure that the position of apogee is not severely affected by the perturbations due to the oblate nature of the Earth. Using the Gauss form of the Lagrange Planetary Equations, in terms of a spacecraft centred RTN coordinate system [6]. The rate of change of argument of perigee is written as,

$$\begin{aligned}\frac{d\omega}{d\theta}=\frac{r^2}{\mu e}&\left[-RCos\theta+T\left(1+\frac{r}{p}\right)Sin\theta\right]\\&-\frac{r^3}{\mu pTani}Sin(\theta+\omega)N\end{aligned} \qquad [5]$$

The disturbing force components due to J_2 [7] are,

$$R_{J_2}=\frac{3}{2}\frac{J_2\mu R_e^{\ 2}}{r^4}(3Sin^2iSin^2(\theta+\omega)-1) \qquad [6]$$

$$T_{J_2}=-\frac{3}{2}\frac{J_2\mu R_e^{\ 2}}{r^4}Sin^2iSin2(\theta+\omega) \qquad [7]$$

$$N_{J_2}=-\frac{3}{2}\frac{J_2\mu R_e^{\ 2}}{r^4}Sin2iSin(\theta+\omega) \qquad [8]$$

Substituting Equations [6] through [8] into Equation [5] and integrating over one orbital revolution results in the well known expression for the change in argument of perigee,

$$\left(\Delta\omega\right)_0^{2\pi}=\frac{3J_2\pi R_e^{\ 2}(3+5Cos2i)}{4a^2(-1+e^2)^2} \qquad [9]$$

To determine the inclination, Equation [9] is set to zero, and solved resulting in critical inclination values of *63.4deg* and *116.6deg*. Thus all orbits with an inclination of *63.4deg* show no rotation of the apsidal line, irrespective of the values of semi-major axis and eccentricity. If inclination is less than *63.4deg* the rotation is eastward and if greater than *63.4deg* the rotation is westward.

IV. LOW-THRUST PROPULSION

Low-thrust terms were added to the disturbing force components, using locally optimal control laws [8] to determine the distinct position on the orbit the sign of the thrust is required to switch direction. The combined J_2 and low-thrust perturbations in each direction are thus,

$$R_{J_2+F_r} = \frac{3}{2}\frac{J_2\mu R_e^2}{r^4}(3Sin^2 iSin^2(\theta+\omega)-1) + F_r \operatorname{sgn}[Cos\theta] \quad [10]$$

$$T_{J_2+F_t} = -\frac{3}{2}\frac{J_2\mu R_e^2}{r^4}Sin^2 iSin2(\theta+\omega) + F_t \operatorname{sgn}[Sin\theta] \quad [11]$$

$$N_{J_2+F_n} = -\frac{3}{2}\frac{J_2\mu R_e^2}{r^4}Sin2iSin(\theta+\omega) + F_n \operatorname{sgn}[Sin(\theta+\omega)] \quad [12]$$

Noting that the orbital radius can be defined as,

$$r = \frac{p}{1+eCos\theta} \quad [13]$$

Thereafter the low-thrust term was included in each direction individually before consideration was given to combining thrust in multiple directions.

Radial Direction

The change in argument of perigee over one orbital revolution, applying continuous radial low-thrust is,

$$(\Delta\omega)_0^{2\pi} = \int_0^{2\pi}\frac{r^2}{\mu e}\left(-R_{J_2+F_r}Cos\theta + T_{J_2}\left(1+\frac{r}{p}\right)Sin\theta\right) - \int_0^{2\pi}Cosi\frac{\sin(\theta+\omega)r^3}{\mu pSini}N_{J_2} \quad [14]$$

Substituting the appropriate perturbation expressions from Equations [10], [7] and [8] respectively gives,

$$\begin{aligned}(\Delta\omega)_0^{2\pi} = &-\frac{3J_2R_e^2}{2p^2e}\int_0^{2\pi}Cos\theta(1+eCos\theta)^2(3Sin^2 iSin^2(\theta+\omega)-1)d\theta \\ &-\frac{p^2F_r}{\mu e}\int_0^{2\pi}\frac{Cos\theta}{(1+eCos\theta)^2}\operatorname{sgn}[Cos\theta]d\theta \\ &-\frac{3}{2}\frac{J_2R_e^2Sin^2 i}{ep^2}\int_0^{2\pi}(Sin\theta(1+eCos\theta)^2\left(1+\frac{1}{1+eCos\theta}\right) \\ &Sin2(\theta+\omega))d\theta \\ &+\frac{3J_2\pi R_e^2Cos^2 i}{p^2}\int_0^{2\pi}\frac{Sin^2(\theta+\omega)}{(1+eCos\theta)^3}d\theta\end{aligned} \quad [15]$$

Integrating Equation [15] over one orbit, recognizing the low-thrust term switches sign depending on *Cos(θ)*, meaning it changes sign at both *θ = 90deg* and *θ = 270deg*. The expression for the change in argument of perigee, using the assumptions that the eccentricity is not equal to either zero or one, is then,

$$\begin{aligned}(\Delta\omega)_0^{2\pi} = &\frac{3J_2\pi R_e^2(3+5Cos2i)}{4a^2(-1+e^2)^2} \\ &+\frac{1}{e\mu}2a^2F_r(2-2e^2+4e\sqrt{-1+e^2}ArcTanh\left[\frac{-1+e}{\sqrt{-1+e^2}}\right] \\ &+e\sqrt{-1+e^2}Log\left[\frac{1-e}{\sqrt{-1+e^2}}\right]-e\sqrt{-1+e^2}Log\left[\frac{-1+e}{\sqrt{-1+e^2}}\right])\end{aligned} \quad [16]$$

Transverse Direction

The change in argument of perigee when a transverse thrust is applied can be written as,

$$(\Delta\omega)_0^{2\pi} = \int_0^{2\pi}\frac{r^2}{\mu e}\left(-R_{J_2}Cos\theta + T_{J_2+F_t}\left(1+\frac{r}{p}\right)Sin\theta\right)d\theta - \int_0^{2\pi}Cosi\frac{Sin(\theta+\omega)r^3}{\mu pSini}N_{J_2}d\theta \quad [17]$$

Substituting in perturbation expressions from Equations [6], [11] and [8] gives,

$$\begin{aligned}(\Delta\omega)_0^{2\pi} = &\frac{-3J_2R_e^2}{2ep^2}\int_0^{2\pi}Cos\theta(1+eCos\theta)^2(3Sin^2 iSin^2(\theta+\omega)-1)d\theta \\ &+\frac{3J_2\pi R_e^2Cos(i)^2}{p^2}\int_0^{2\pi}\frac{Sin(\theta+\omega)^2}{(1+eCos\theta)^3}d\theta \\ &-\frac{3J_2R_e^2Sin^2 i}{ep^2}\int_0^{2\pi}(1+eCos\theta)^2Sin2(\theta+\omega)\left(1+\frac{1}{1+eCos\theta}\right)d\theta \\ &+\frac{p^2}{\mu e}\int_0^{2\pi}\frac{Sin\theta F_t\operatorname{sgn}[Sin\theta]}{(1+eCos\theta)^2}\left(1+\frac{1}{1+eCos\theta}\right)d\theta\end{aligned} \quad [18]$$

Noting, that the transverse low-thrust term switches sign as a function of *Sin(θ)*, thus in this case changes sign at *θ = 180deg*. Integrating Equation [18] using the assumption that the eccentricity is again between zero and one, results in,

$$(\Delta\omega)_0^{2\pi}=\frac{3J_2\pi R_e^2\left(3+5Cos2i\right)}{4a^2\left(-1+e^2\right)^2}-\frac{4a^2(-2+e^2)F_t}{e\mu} \quad [19]$$

Normal Direction

Unlike the low-thrust perturbations in the radial and transverse directions, the normal low-thrust switches sign as a function of argument of latitude. Consequently, the value assigned to the argument of perigee becomes important in this case, making the normal low-thrust case significantly more complex. The study therefore considered the maximum and minimum of the problem, solving for low-thrust using argument of perigee equal to both *0deg* and *90deg*.

The general expression for the change in argument of perigee with normal low-thrust is,

$$\begin{aligned}(\Delta\omega)_0^{2\pi}&=\int_0^{2\pi}\frac{r^2}{\mu e}\left(-R_{J_2}Cos\theta+T_{J_2}\left(1+\frac{r}{p}\right)Sin\theta\right)d\theta \\ &-\int_0^{2\pi}Cosi\frac{Sin(\theta+\omega)r^3}{\mu pSini}N_{J_2+F_n}d\theta\end{aligned} \quad [20]$$

Again, substituting appropriate expressions for the disturbing forces, Equation [20] becomes,

$$\begin{aligned}(\Delta\omega)_0^{2\pi}&=\frac{-3J_2R_e^2}{2ep^2}\int_0^{2\pi}Cos\theta(1+eCos\theta)^2(3Sin^2iSin^2(\theta+\omega)-1)d\theta \\ &-\frac{3}{2}\frac{J_2R_e^2Sin^2i}{ep^2}\int_0^{2\pi}(Sin\theta(1+eCos\theta)^2\left(1+\frac{1}{1+eCos\theta}\right) \\ &Sin2(\theta+\omega))d\theta \\ &+\frac{3J_2\pi R_e^2Cos^2i}{p^2}\int_0^{2\pi}\frac{Sin^2(\theta+\omega)}{(1+eCos\theta)^3}d\theta \\ &-\frac{p^2CosiF_n}{\mu Sini}\int_0^{2\pi}\frac{Sin(\theta+\omega)}{(1+eCos\theta)^3}\text{sgn}[Sin(\theta+\omega)]d\theta\end{aligned} \quad [21]$$

ω = 0 deg

Locally optimal control laws show that the normal low-thrust term switches direction as a function of $Sin(\theta+\omega)$. Thus if the argument of perigee is set to zero, the argument of latitude reduces to the true anomaly, so low-thrust switches sign at θ = *180deg*. Integrating Equation [21] over one orbital revolution, using the same assumptions as previous integrations results in,

$$(\Delta\omega)_0^{2\pi}=\frac{3J_2\pi R_e^2\left(3+5Cos2i\right)}{4a^2\left(-1+e^2\right)^2}-\frac{4a^2F_nCos\omega Coti}{\mu} \quad [22]$$

ω = 90 deg

When argument of perigee is set to *90deg*, locally optimal control laws show that the normal component of thrust must still change sign at an argument of latitude of *180deg*. Integrating over one orbit, and again making the assumption that eccentricity is not equal to zero or one produces the expression,

$$\begin{aligned}(\Delta\omega)_0^{2\pi}&=\frac{3J_2\pi R_e^2\left(3+5Cos2i\right)}{4a^2\left(-1+e^2\right)^2} \\ &+\frac{1}{\sqrt{-1+e^2}\mu}a^2F_nCoti(4\sqrt{-1+e^2}+2e^2\sqrt{-1+e^2} \\ &-12eArcTanh\left[\frac{-1+e}{\sqrt{-1+e^2}}\right]-3eLog\left[\frac{1-e}{\sqrt{-1+e^2}}\right] \\ &+3eLog\left[\frac{-1+e}{\sqrt{-1+e^2}}\right])Sin\omega\end{aligned} \quad [23]$$

Equations [16], [19], [22] and [23], were solved analytically, using the orbital elements shown in Table 1 to determine the value of low-thrust required to reach a range of inclinations between *5deg* and *175deg*.

Table 1 Molniya Orbital Elements

Orbital Element	Value	
Perigee Altitude	813.2	[km]
Apogee Altitude	39539.7	[km]
Ascending Node	329.6	[deg]
Argument of perigee	270	[deg]

Figure 1 plots the results of solving for low-thrust for a given inclination in the radial, transverse and normal directions.

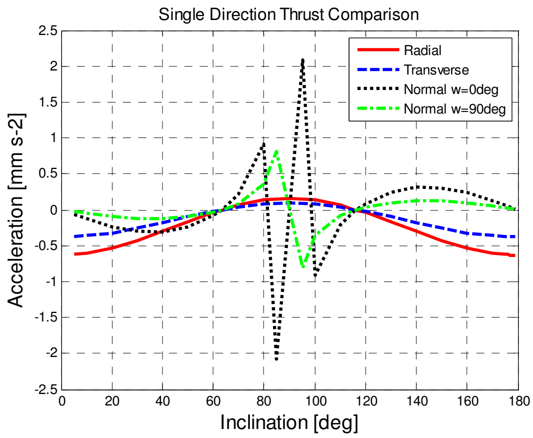

Figure 1 Single direction thrust comparison

Figure 1 shows the required acceleration using low-thrust propulsion in any of the radial, transverse or normal directions to change the critical inclination of the orbit to a wide range of possible values.

It is shown that thrusting in the transverse direction allows any inclination to be reached using the lowest acceleration magnitude in any of the single directions, for example an inclination of *90deg* is possible using a thrust of *0.0942 mm* s^{-2}. It is also noted that a singularity occurs at an inclination of *90deg* when thrusting in the normal direction. The reason for this is explained by examination of Equations [22] and [23], where it is shown that the low-thrust term in these equations contains the expression *Cot(i)*. At *i* equal to *90deg Cot(i)* becomes undefined, causing the singularity.

V. COMBINED LOW-THRUST

The possibility of combining an equal and constant magnitude of low-thrust in two of the axial directions was examined to confirm if the spacecraft could reach a given inclination with a lower acceleration magnitude than in any single direction.

Radial and Transverse Thrust

The expression for the change in argument of perigee when radial and transverse thrusts are combined is,

$$(\Delta\omega)_0^{2\pi} = \int_0^{2\pi}\frac{r^2}{\mu e}\left(-R_{J_2+F_r}Cos\theta + T_{J_2+F_t}\left(1+\frac{r}{p}\right)Sin\theta\right)d\theta - \int_0^{2\pi} Cosi\frac{Sin(\theta+\omega)r^3}{\mu pSini}N_{J_2}d\theta \quad [24]$$

Substituting the perturbation equations into Equation [24] gives,

$$\begin{aligned}(\Delta\omega)_0^{2\pi} = &-\frac{3J_2R_e^2}{2p^2e}\int_0^{2\pi}Cos\theta(1+eCos\theta)^2(3Sin^2iSin^2(\theta+\omega)-1)d\theta \\ &-\frac{3}{2}\frac{J_2R_e^2Sin^2i}{ep^2}\int_0^{2\pi}(Sin\theta(1+eCos\theta)^2\left(1+\frac{1}{1+eCos\theta}\right) \\ &Sin2(\theta+\omega))d\theta \\ &+\frac{3J_2\pi R_e^2Cos^2i}{p^2}\int_0^{2\pi}\frac{Sin^2(\theta+\omega)}{(1+eCos\theta)^3}d\theta \\ &-\frac{p^2F_r}{\mu e}\int_0^{2\pi}\frac{Cos\theta}{(1+eCos\theta)^2}\operatorname{sgn}[Cos\theta]d\theta \\ &+\frac{p^2}{\mu e}\int_0^{2\pi}\frac{Sin\theta F_t\operatorname{sgn}[Sin\theta]}{(1+eCos\theta)^2}\left(1+\frac{1}{1+eCos\theta}\right)d\theta\end{aligned} \quad [25]$$

Integrating over one orbital revolution, again using the assumption that the eccentricity was between 0 and 1, gives the change in argument of perigee as,

$$\begin{aligned}(\Delta\omega)_0^{2\pi} = &\frac{1}{e\mu}2a^2F_r(2-2e^2+4e\sqrt{-1+e^2}ArcTanh\left[\frac{-1+e}{\sqrt{-1+e^2}}\right] \\ &+e\sqrt{-1+e^2}Log\left[\frac{1-e}{\sqrt{-1+e^2}}\right]-e\sqrt{-1+e^2}Log\left[\frac{-1+e}{\sqrt{-1+e^2}}\right]) \\ &-\frac{4a^2\left(-2+e^2\right)F_t}{e\mu}+\frac{3J_2\pi R_e^2\left(3+5Cos2i\right)}{4a^2\left(-1+e^2\right)^2}\end{aligned} \quad [26]$$

When combining the forces in multiple directions it was assumed that the magnitude of thrust in each direction was the same. This made it possible to analytically solve Equation [26], for low-thrust, again using the value of orbital elements from Table 1. The results of the total thrust required to reach inclinations between *5deg* and *175deg* are shown in Figure 2, the individual radial and transverse thrusts are also plotted for comparison.

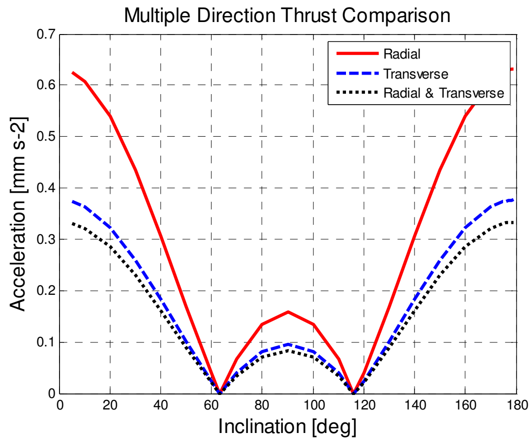

Figure 2 Combined Thrust Comparison

Only the magnitude of the individual thrusts is plotted in order to make comparison with the combined thrust easier. Results showed that combining the radial and transverse thrusts in this way, allowed a reduction in acceleration magnitude to achieve any inclination between *5 deg* and *175 deg*.

It is noted that making the assumption that the thrust magnitude is the same in each direction means the solution is not optimal. At some points in the orbit it would be beneficial to thrust only in one direction, and around the orbit the fraction of the total force in each direction would change depending on the true anomaly, for this reason assuming the same fraction of the total force in each direction does not produce an optimal solution. Nonetheless, it was possible to combine low-thrust in radial and transverse directions to produce a reduction in the amount of thrust needed to get to any given inclination.

The same is not always true when combining the low-thrust in the normal direction with either the radial or transverse directions. The reason being that the low-thrust expressions in Equations [22] and [23] include a *Cot(i)* term, meaning the value of this term changes depending on the value of inclination to be achieved. The combined thrust is therefore sometimes lower than individual thrusts, depending on the value of inclination. The assumption that the fraction of the total force was equal in each direction again meant that the solution was not optimal, as it is again being forced to act in multiple directions at points where thrusting in just a single direction would be more beneficial.

VI. CHANGE IN ORBITAL ELEMENTS

Using the Gauss form of the Lagrange Planetary Equations, in terms of a spacecraft centred RTN coordinate system [6], the change in orbital elements due to the applied low-thrust were obtained analytically to show that the desired zero secular rate of change of other elements has been maintained.

Semi-Major Axis

$$\frac{da}{d\theta}=\frac{2pr^2}{\mu\left(1-e^2\right)^2}\left(R_{J_2+F_r}eSin\theta+T_{J_2+F_t}\frac{p}{r}\right) \quad [27]$$

Substituting the appropriate expressions for perturbing forces gives,

$$\begin{aligned}\frac{da}{d\theta}=&\frac{1}{\mu\left(1+eCos\theta\right)^2}2a^3\left(1-e^2\right) \quad [28]\\ &\left(eSin\theta\left(F_r+\frac{3J_2R_e^2\mu\left(1+eCos\theta\right)^4\left(-1+3Sin(i)^2\,Sin(\theta+\omega)^2\right)}{2a^4\left(1-e^2\right)^4}\right)\right.\\ &\left.+\left(1+eCos\theta\right)\left(F_t-\frac{3J_2R_e^2\mu\left(1+eCos\theta\right)^4\,Sin(i)^2\,Sin\left(2(\theta+\omega)\right)}{2a^4\left(1-e^2\right)^4}\right)\right)\end{aligned}$$

Integrating Equation [28] over one orbital revolution and switching the sign of radial and transverse thrusts at the positions defined previously using locally optimal control laws, results in,

$$\left(\Delta a\right)_0^{2\pi}=0 \quad [29]$$

Eccentricity

$$\frac{de}{d\theta}=\frac{r^2}{\mu p}\left(R_{J_2+F_r}Sin\theta+T_{J_2+F_r}\left(\left(1+\frac{r}{p}\right)Cos\theta+\frac{re}{p}\right)\right) \quad [30]$$

Substituting the radial and transverse disturbing forces gives the rate of change of argument of perigee as,

$$\begin{aligned}\frac{de}{d\theta}=&\frac{1}{\mu\left(1+eCos\theta\right)^2}a\left(1-e^2\right)(Sin\theta(F_r\\ &+\frac{3J_2R_e^2\mu\left(1+eCos\theta\right)^4\left(-1+3Sin(i)^2\,Sin(\theta+\omega)^2\right)}{2a^4\left(1-e^2\right)^4})) \quad [31]\\ &+\left(\frac{e}{1+eCos\theta}+Cos\theta\left(1+\frac{1}{1+eCos\theta}\right)\right)\\ &\left(F_t-\frac{3J_2R_e^2\mu\left(1+eCos\theta\right)^4\,Sin(i)^2\,Sin\left(2(\theta+\omega)\right)}{2a^4\left(1-e^2\right)^4}\right)\end{aligned}$$

Integrating over one orbit, switching the sign of low-thrust terms as appropriate, gives the change in eccentricity,

$$\left(\Delta e\right)_0^{2\pi}=0 \quad [32]$$

Inclination

$$\frac{di}{d\theta}=\frac{r^3}{\mu p}Cos\left(\theta+\omega\right)N_{J_2+F_n} \quad [33]$$

Using the expression for the normal perturbation, Equation [33] becomes,

$$\frac{di}{d\theta}=\frac{a^2\left(1-e^2\right)^2 Cos\left(\theta+\omega\right)}{\mu\left(1+eCos\theta\right)^3} \left(F_n-\frac{3J_2R_e^2\mu\left(1+eCos\theta\right)^4 Sin\left(2i\right)Sin\left(\theta+\omega\right)}{2a^4\left(1-e^2\right)^4}\right) \quad [34]$$

Once more, locally optimal control laws state that normal thrust switches sign depending on the argument of latitude, therefore Equation [34] is solved using $\omega = 0deg$ and $\omega = 90deg$.

ω = 0deg

Integrating Equation [34] over one orbital revolution,

$$\left(\Delta i\right)_0^{2\pi}=-\frac{4a^2F_nSin\omega}{\mu} \quad [35]$$

Substituting in values of orbital elements results in,

$$\left(\Delta i\right)_0^{2\pi}=0 \quad [36]$$

ω = 90deg

Change in inclination when argument of perigee is *90deg* is,

$$\left(\Delta i\right)_0^{2\pi}=\frac{1}{\sqrt{-1+e^2}\mu}a^2F_nCos\omega(4\sqrt{-1+e^2}+2e^2\sqrt{-1+e^2} -12eArcTanh\left[\frac{-1+e}{\sqrt{-1+e^2}}\right]-3eLog\left[\frac{1-e}{\sqrt{-1+e^2}}\right] +3eLog\left[\frac{-1+e}{\sqrt{-1+e^2}}\right]) \quad [37]$$

Inserting values of orbital elements, gives the change in inclination as,

$$\left(\Delta i\right)_0^{2\pi}=0 \quad [38]$$

Ascending Node Angle

$$\frac{d\Omega}{d\theta}=\frac{r^3}{\mu pSini}Sin\left(\theta+\omega\right)N_{J_2+F_n} \quad [39]$$

Inserting the expressions for the normal perturbation results in,

$$\frac{d\Omega}{d\theta}=\frac{a^2\left(1-e^2\right)^2 Sin\left(\theta+\omega\right)}{Sini\left(1+eCos\theta\right)^3} \left(F_n-\frac{3J_2R_e^2\mu\left(1+eCos\theta\right)^4 Sin\left(2i\right)Sin\left(\theta+\omega\right)}{2a^4\left(1-e^2\right)^4}\right) \quad [40]$$

The change in ascending node angle was calculated using both $\omega = 0deg$ and $\omega = 90deg$.

Ω = 0deg

Change in ascending node over one orbital revolution,

$$\left(\Delta\Omega\right)_0^{2\pi}=\frac{4a^2F_nCos\omega}{\mu Sini}-\frac{3J_2\pi R_e^2Cosi}{a^2\left(-1+e^2\right)^2} \quad [41]$$

Including values of orbital elements, as previously specified, does produce a change in ascending node angle. However, this value is of the same magnitude as the drift experienced when no low-thrust is applied to the natural Molniya orbit and is therefore of an acceptable level.

Ω = 90deg

Integrating Equation [40] over one orbit gives,

$$\left(\Delta\Omega\right)_0^{2\pi}=-\frac{1}{2a^2\left(-1+e^2\right)^{5/2}\mu Sini}(3\sqrt{-1+e^2}J_2\pi R_e^2\mu Sin\left(2i\right)+ 24a^4e\left(-1+e^2\right)^2F_nArcTanh\left[\frac{-1+e}{\sqrt{-1+e^2}}\right]Sin\omega -2a^4\left(-1+e^2\right)^2F_n)(2\sqrt{-1+e^2}\left(2+e^2\right) -3eLog\left[\frac{1-e}{\sqrt{-1+e^2}}\right]+3eLog\left[\frac{-1+e}{\sqrt{-1+e^2}}\right])Sin\omega \quad [42]$$

Again substituting in values for parameters results in a small drift in ascending node, again of the same magnitude as the change experienced for the natural Molniya orbit.

VII. NUMERICAL SIMULATION

Analytical results were validated using a numerical simulation. The numerical simulation used the analytical results as the input and produced the changes in all orbital elements for a given number of orbital revolutions.

The numerical model propagated the spacecraft position, by integrating the Gauss form of the Lagrange Planetary Equations, using an explicit, variable step size Runge Kutta (4,5) formula, the Dormand-Price pair (a single step method) [9]. Numerical simulations included perturbations only due to Earth oblateness, to the order of J_2 only, and results were found to validate the analytical expressions. The numerical model proved that not only was the change in argument of perigee negligible due to the applied low-thrust, but the change in all other orbital elements also matched the analytical results.

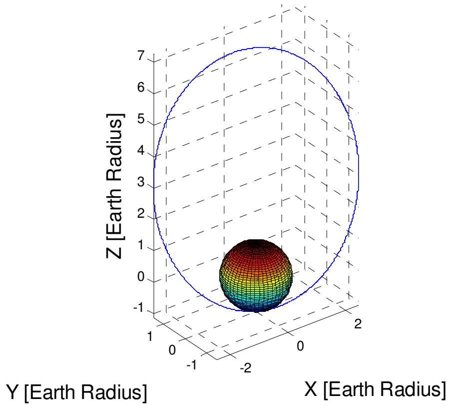

Figure 3: Orbit propagation for applied radial and transverse low-thrust over seven orbital revolutions

Figure 3 shows the propagation of seven orbits at an initial inclination of *90 deg* with an applied radial and transverse low-thrust, with a total magnitude of $0.0834\ mm\ s^{-2}$.

Figure 3 illustrates that after seven orbital revolutions, the spacecraft still returns to its original position and follows the same orbit.

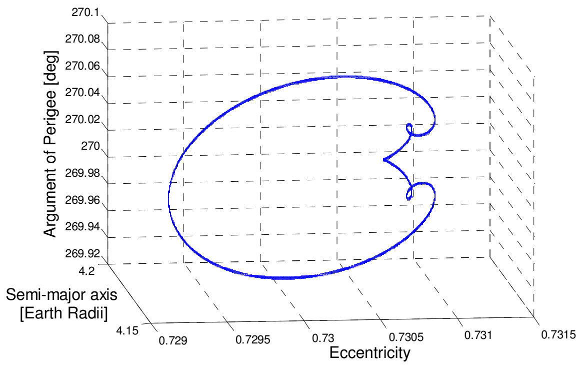

Figure 4 Change in orbital elements

Figure 4 illustrates the variation in orbital elements over seven orbital revolutions. Examination of the plot shows that although semi-major axis, eccentricity and argument of perigee vary during one orbit, all orbital elements return to the same initial value. Plotting inclination and ascending node angle showed no variation of these parameters over an orbital revolution. The same process was conducted for each direction of thrust individually and the spacecraft again returned to its original position after seven orbital revolutions.

VIII. DISCUSSION

Results show that it is possible to use low-thrust propulsion to change the critical inclination of the Molniya orbit to enable new Earth Observation orbits. The most significant finding was the ability to change the inclination to *90deg*, to enable a Polar-Molniya orbit. Such an orbit is facilitated, by applying continuous low-thrust in the radial and transverse directions. The acceleration required to allow such a modification in orbit inclination is small and, for example, using 1000kg spacecraft the necessary thrust is less than 85mN, which can easily be achieved using existing technology such as ion engines. One example is the QinetiQ T6 thruster, which has the ability to provide 50-230 mN at a specific impulse above 4500 seconds for the BepiColombo mission [10].

In creating a Polar-Molniya orbit, the spacecraft spends a large amount of time above the Arctic Circle, as a result of apogee dwell; this is beneficial for many reasons. Particularly for Earth Observation missions as the Arctic is a rapidly changing environment where at the North Pole the effects of climate change are both amplified and accelerated. Observations are also vital to monitor the rapidly diminishing ice cover, and changing snow in this region. In addition to this, the Arctic Circle is of high meteorological and climate significance, as the weather has an impact on global weather and climate prediction, as well as being a significant region for volcanic ash transport and air pollution. There is also an increasing demand for communication and data relay in the remote polar-regions. Since communication is typically conducted using spacecraft in Geostationary orbits (GEO) at latitudes above *70deg-72deg* it becomes impractical to use GEO satellites for communication [3]. It is therefore imperative that means of ensuring reliable, secure communications in the Arctic are obtained. With increasing economic activity in this region due to resource exploration and development and increased marine and air traffic all of these areas become significant.

Traditionally, observation of the Earths poles is conducted using a Sun-synchronous Polar orbit, a spacecraft on such an orbit circles the Earth around fourteen times per day [11]. During which time, Earth imaging is conducted taking measurements over a strip several tens to hundreds of kilometres wide, building up an image of a particular location. For example Landsat 7 has a sixteen day Earth coverage cycle*, meaning that the adjacent swath to the west of a previous swath is travelled by Landsat 7 one week later (and the adjacent swath to the east occurred one week earlier and will recur nine days later). The problem associated with these polar orbits is that the temporal resolution provided is insufficient. Temporal resolution is improved using satellites on a geostationary orbit; however these geostationary systems are unable to view deep Polar Regions. Hence, imaging of Polar Regions has in the past been achieved by creating a mosaic of both satellite images [12]. This process gives a general summary of weather patterns for a period, but does not give a completely accurate representation, as the image is not continuous. The Molniya orbit overcomes some of the problems associated with imaging of high latitude regions, as a spacecraft on this orbit spends a large amount of time over the Arctic Circle. However, the accuracy of data of this region can be further improved using the Polar-Molniya orbit due to the increased inclination of this orbit. Over and above more consistent and accurate Earth imaging, secure and dependable communications in high latitude regions is also facilitated using the Polar-Molniya orbit.

The low-altitude of the conventional Sun-synchronous Polar orbiting spacecraft means in order to achieve real time continuous observation of the Earth, a constellation of between thirty and one hundred spacecraft are required [13]. An alternative to the Sun-synchronous orbit for polar observation is a hybrid solar sail and Solar Electric Propulsion (SEP) system stationed at an artificial Lagrange point above one of the Earth's poles [14]. This configuration gives complete hemispherical views throughout the year, however to achieve this, the spacecraft must be positioned around 3million km above the Earth's surface. The conventional Molniya orbit spends a large amount of time at apogee above the Northern hemisphere, allowing satisfactory observation of this region. However, by using low-thrust propulsion to change the critical inclination to enable a Polar-Molniya orbit, apogee is now directly above the Arctic Circle. This higher inclination means the spacecraft can view the North Pole for longer periods of time; consequently, continuous hemispherical observation can be achieved using only three spacecraft. The Polar-Molniya orbit therefore offers continuous observation of the North Pole with fewer spacecraft than Sun-synchronous and traditional Molniya orbits, and at a higher resolution that a hybrid solar sail and SEP system at an artificial Lagrange point stationed above the pole.

* NASA's Landsat 7 Science Data Users Handbook, 1998

IX. FUTURE WORK

Scope for significant future work in this area exists, with the first step aiming to achieve numerically optimal solutions. The assumption that the magnitude of thrust was the same in each direction would no longer be made; hence a fuel optimal solution could be determined.

Further work would also include the addition of higher order Earth harmonic terms into the numerical model, and the inclusion of other perturbations such as atmospheric drag, third body effects and solar radiation pressure, all of which would increase the accuracy of the results.

Supplementary work may include mission durations, analysis of the technology required, stability and control in addition to investigation into scientific applications of the work.

X. CONCULSION

The results of the study illustrated the feasibility of using low-thrust propulsion to alter the critical inclination of the Molniya orbit. It was shown that this could be achieved while maintaining the zero change in argument of perigee condition fundamental to this orbit, and ensuring other orbital elements were not adversely affected by the applied low-thrust.

The study examined the application of low-thrust in radial, transverse and normal directions individually, before consideration was given to combining the thrust in multiple directions. It was found that thrusting in the transverse direction enabled the orbit inclination to be changed to any value using the lowest magnitude of acceleration in any single direction However; it was found that this value was further reduced when radial and transverse thrusts were combined. It was found that combining the thrust in the normal direction with either the radial or transverse thrusts, did not necessarily reduce the thrust required to achieve a certain inclination.

In varying the critical inclination of the Molniya orbit, the potential applications are extended. The major application is enabling a Polar-Molniya orbit by changing the inclination to *90deg*. As such continuous, real-time imaging of the Arctic Circle is enabled using existing or near-term technology. The potential applications of such an orbit include, opportunities for reliable communications in high latitude regions, previously unfeasible using satellites on a geostationary orbit, real-time observation of the Arctic Region using fewer spacecraft than traditional Sun-synchronous orbits, and more accurate imaging by removing the inaccuracy of piecing together a mosaic image of a particular location from geostationary and polar orbit data. This allows an improvement in climate and weather data for the rapidly changing environment of the Arctic Region.

XI. ACKNOWLEDGEMENTS

This work was part funded by NERC grant reference number NE/1000801/1;SpeCL: Early Concepts for a New Mission: A Spaceborne Multispectral Canopy Lidar.

XII. REFERENCES

[1] "Global Monitoring of Essential Climate Variables," in *ESA/PB-EO(2009)32*, ed: Esa-Earth Observation Programme Board.

[2] M. Macdonald*, et al.*, "Extension of the Sun-Synchronous Orbit," *Journal Guidance Control and Dynamics,* vol. In Press, 2010.

[3] J. R. Wertz, *Mission Geometry: Orbit and Constellation Design and Management*, 2001.

[4] S. Q. Kidder and T. H. Vonder Haar, "On the Use of Molniya Orbits for Meteorological Observation of Middle and High Latitudes," *Journal of Atmospheric and Oceanic Technology,* vol. 7, pp. 517-522, 1990.

[5] R. R. Bate*, et al.*, *Fundamentals of Astrodynamics*: Dover Publications, Inc, 1971.

[6] P. Fortescue*, et al.*, *Spacecraft Systems Engineering*, Third ed., 2003.

[7] D. A. Vallado, *Fundamentals of Astrodynamics and Applications*, Third ed., 2001.

[8] M. Macdonald and C. R. McInnes, "Analytical Control Laws for Planet-Centered Solar Sailing," *Journal of Guidance, Control and Dynamics,* vol. 28, pp. 1038-1048, September - October 2005 2005.

[9] J. R. Dormand and P. J. Prince, "A family of embedded Runge-Kutta formulae," *Journal of Computational and Applied Mathematics and Statistics,* vol. 6, pp. 19-26, 1980 1980.

[10] N. C. Wallace, "Testing of The QinetiQ T6 Thruster in Support of the ESA BepiColombo Mercury Mission," in *4th International Spacecraft Propulsion Conference (ESA SP-55)*, Cagliari, Sardinia, Italy, 2004.

[11] R. J. Boain, "A-B-Cs of Sun-Synchronous Orbit Mission Design," presented at the 14th AAS/AIAA Space Flight Mechanics Conference, Maui, Hawaii, 2004.

[12] M. A. Lazzara*, et al.*, "10 Years of Antarctic Composite Images."

[13] T. J. Lang, "Optimal Low Earth Orbit Constellations for Continuous Global Coverage," in *AAS/AIAA Astrodynamics Conference*, Victoria, Canada, 1993, pp. 1199-1216.

[14] M. Ceriotti and C. R. McInnes, "A Near Term Pole-Sitter using Hybrid Solar Sail Propulsion," presented at the 2nd International Symposium on Solar Sailing, New York, USA, 2010.